American Journal of Energy Engineering
2026, Vol. 14, No. 3, pp. 108–116
https://doi.org/10.11648/j.ajee.20261403.12

SciencePG
Science Publishing Group

Research Article

Multicomponent Iridium-Based Alloy Catalysts for Enhanced Alkaline Hydrogen Oxidation Reaction

Yanfu Tong, Zhiyuan Liu, Xuejin Li, Wei Xing*

Shandong Key Laboratory of Intelligent Energy Materials, School of Materials Science and Engineering, China University of Petroleum (East China), Qingdao, China

Abstract

The sluggish kinetics of the hydrogen oxidation reaction (HOR) in alkaline media, primarily arising from the linear scaling relationship between H* and OH* adsorption energies on catalyst surfaces, remains a critical bottleneck for anion-exchange membrane fuel cells (AEMFCs). In this study, we propose a multifaceted approach to overcoming the current limitations of scaling by synthesising Ir-based ternary alloys with diverse oxophilic metals, including Mo, Ru, and Nb. The RuIrMo@MHCS catalyst, featuring a face-centred cubic single-phase solid solution with uniformly dispersed nanoparticles on hollow carbon spheres, exhibits a kinetic current density of 18.04 mA cm^{-2} at 50 mV overpotential and an exchange current density of 6.79 mA cm^{-2}. This is a significant improvement over the performance of commercial Pt/C, with factors of 6.14 and 5.66, respectively. Additionally, the catalyst demonstrates excellent long-term stability. X-ray photoelectron spectroscopy reveals electron transfer from Ir to Ru upon Ru doping. Density functional theory calculations demonstrate that Ru incorporation downshifts the d-band centre of Ir, thereby moderately weakening H* adsorption ($\Delta G_{H^*} = -0.38$ eV) while enhancing OH* adsorption on Mo sites. This adaptable calibration of intermediate adsorption energies circumvents the linear scaling constraint and substantially promotes alkaline HOR kinetics. The findings of this study corroborate the hypothesis that multicomponent alloying is an effective strategy for synergistic optimisation of H* and OH* binding, thus providing a rational design pathway for high-performance alkaline HOR catalysts.

Keywords

Alkaline Hydrogen Oxidation Reaction, Iridium-based Catalyst, Multicomponent Alloy

1. Introduction

The transition to a low-carbon energy economy has positioned hydrogen as a promising energy carrier, with fuel cells playing a central role in efficient hydrogen utilization. Among various fuel cell technologies, anion-exchange membrane fuel cells (AEMFCs) offer distinct advantages, including the potential use of non-precious metal catalysts, reduced corrosion, and lower system costs [1-3]. However, the commercialization of AEMFCs is hindered by the intrinsically sluggish kinetics of the hydrogen oxidation reaction (HOR) in alkaline media, which is two to three orders of magnitude slower than that in acidic electrolytes on state-of-the-art Pt-based catalysts [4, 5].

The origin of this kinetic limitation lies in the more complex

*Correspondence: Wei Xing (xingwei@upc.edu.cn)

Received: 25 May 2026; **Accepted:** 25 June 2026; **Published:** 6 August 2026

reaction mechanism in alkaline conditions. Unlike in acid where HOR proceeds via H* intermediates only, the alkaline HOR involves both H* and OH* species, typically following Tafel–Volmer or Heyrovsky–Volmer pathways [6-8]. The widely accepted bifunctional theory suggests that an ideal alkaline HOR catalyst should possess balanced adsorption energies for H* and OH: sufficiently strong H binding to enable H_2 dissociation, and adequate OH* affinity to facilitate the Volmer step [9, 10]. Unfortunately, on monometallic surfaces, the adsorption energies of H* and OH* are correlated through a linear scaling relationship, making independent optimization challenging [11]. Binary alloys provide some degree of tunability but remain constrained within a narrow compositional space.

Multicomponent alloys have recently emerged as a promising platform to circumvent scaling relationships [12, 13]. Their multi-element composition creates a distribution of active sites with diverse adsorption properties, allowing H* and OH* binding to be decoupled and optimized separately [14]. Moreover, the increased configurational entropy suppresses phase separation and surface oxidation, enhancing long-term stability.

Iridium-based materials are particularly attractive for alkaline HOR due to their moderate hydrogen binding energy (HBE), strong hydroxyl binding energy (OHBE), and superior CO tolerance compared to Pt [15-18]. Alloying Ir with oxophilic metals such as Ru, Mo, or Nb can further modulate its electronic structure and surface chemistry. In this work, we designed a series of Ir-based multicomponent alloys (IrMo, RuIrMo, and NbIrMo) supported on mesoporous hollow carbon spheres (MHCS). Through comprehensive structural characterization, electrochemical evaluation, and density functional theory (DFT) calculations, we demonstrate that RuIrMo@MHCS exhibits exceptional alkaline HOR activity and stability, with Ru doping inducing a downshift of the Ir d-band center that weakens H* adsorption while preserving strong OH* adsorption – a combination that breaks the linear scaling relation and accelerates reaction kinetics.

2. Materials and Methods

2.1. Synthesis of MHCS Support

The synthesis of mesoporous hollow carbon spheres was accomplished through a one-pot method. Ethanol, deionized water, and aqueous ammonia were mixed in a 7:1:1 volume ratio (total 83 mL) under stirring for 15 min. Tetraethyl orthosilicate (3.46 mL) was added and stirred for a further 15 min, following which 0.4 g of resorcinol and 0.56 mL of formaldehyde (37 wt.%) were added. The mixture was stirred at room temperature for 24 h to allow polymerisation. The product was collected by means of centrifugation, dried in vacuum, and calcined at 700°C for 5 h under N_2. The silica template was removed through the process of etching with a 20 wt.% NaOH solution, thereby yielding MHCS.

2.2. Preparation of Ir-Based Alloy Catalysts

The conventional impregnation-reduction technique was employed in this study. $IrCl_3 \cdot 3H_2O$ (0.04 mmol), $(NH_4)_6Mo_7O_{24} \cdot 4H_2O$ (0.006 mmol), and either $RuCl_3 \cdot 3H_2O$ or $Nb(HC_2O_4)_5$ (0.01 mmol) and MHCS powder (70 mg) were dispersed in 30 mL of deionised water by means of ultrasonication. The suspension was then exposed to ultrasonication for a period of two hours, following which it was subjected to rotary evaporation at a temperature of 80°C. The precursor powder was reduced under H_2/Ar atmosphere at 600°C for 2 h (ramping rate: 5°C/min). The resulting catalysts were denoted RuIrMo@MHCS, NbIrMo@MHCS, and IrMo@MHCS (without the third metal).

2.3. Materials Characterization

X-ray diffraction (XRD) was performed on a Bruker D8 Advance. Scanning electron microscopy (SEM) and transmission electron microscopy (TEM) were conducted on a JEOL JEM-ARM200F and a SEM500. X-ray photoelectron spectroscopy (XPS) used monochromatic Al Kα radiation. Elemental mapping was obtained by energy-dispersive X-ray spectroscopy (EDS).

2.4. Electrochemical Measurements

All tests were performed on a CHI660E electrochemical workstation using a three-electrode system in 0.1 M KOH at room temperature. A glassy carbon rotating disk electrode (RDE, 0.1256 cm^2) was used as the working electrode, with Hg/HgO as reference and Pt wire as counter electrode. Catalyst ink was prepared by dispersing 2 mg catalyst in 980 µL isopropanol and 20 µL Nafion (5 wt.%), then ultrasonicated. The working electrode was loaded with 6 µL of ink (catalyst loading ~12 µg cm^{-2}). Cyclic voltammetry (CV) was recorded at 50 mV s^{-1}. HOR polarization curves were obtained at 5 mV s^{-1} under various rotation speeds (400–3600 rpm) in H_2-saturated electrolyte. All potentials were referenced to reversible hydrogen electrode (RHE) after iR correction. Kinetic current density (j_k) and exchange current density (j_0) were derived from the Koutecky–Levich equation and Butler–Volmer fitting. Chronoamperometry was performed at 0.05 V for stability evaluation. CO stripping was conducted after CO adsorption at 0.05 V for 10 min in CO-saturated KOH.

2.5. DFT Calculations

Density functional theory (DFT) calculations were performed using the CASTEP code within Materials Studio software. The exchange-correlation energy was estimated via the generalized gradient approximation (GGA) employing the Perdew-Burke-Ernzerhof (PBE) functional. Additionally, the DFT-D3 correction was integrated into all computational models to incorporate Van der Waals dispersion interactions.

The simulations were implemented with a plane-wave basis set defined by a energy cutoff of 571.4 eV, and a 4 × 4 × 1 Monkhorst Pack k-point grid was used to integrate the Brillouin zone. The geometry optimization and energy calculation were terminated when the energy, force, stress and displacements reached 1×10^{-5} eV atom^{-1}, 3×10^{-2} eV Å^{-1}, 5×10^{-2} and 1×10^{-3} respectively. Transition state configurations were identified through combined linear/quadratic synchronous transit methodologies, subsequently verified by vibrational frequency analysis.

4. Results and Discussion

4.1. Structural Characterization

SEM and TEM images (Figure 1a and b) reveal that RuIrMo@MHCS maintains the hollow carbon sphere morphology with alloy nanoparticles uniformly dispersed on the surface. High-resolution TEM (Figure 1c) shows lattice fringes with a spacing of 0.214 nm, corresponding to the (111) plane of face-centered cubic Ir, which is slightly contracted compared to pure Ir (0.222 nm) due to Ru/Mo incorporation [19]. EDS elemental mapping (Figure 1d) confirms homogeneous distribution of Ru, Ir, and Mo on the N-doped carbon spheres.

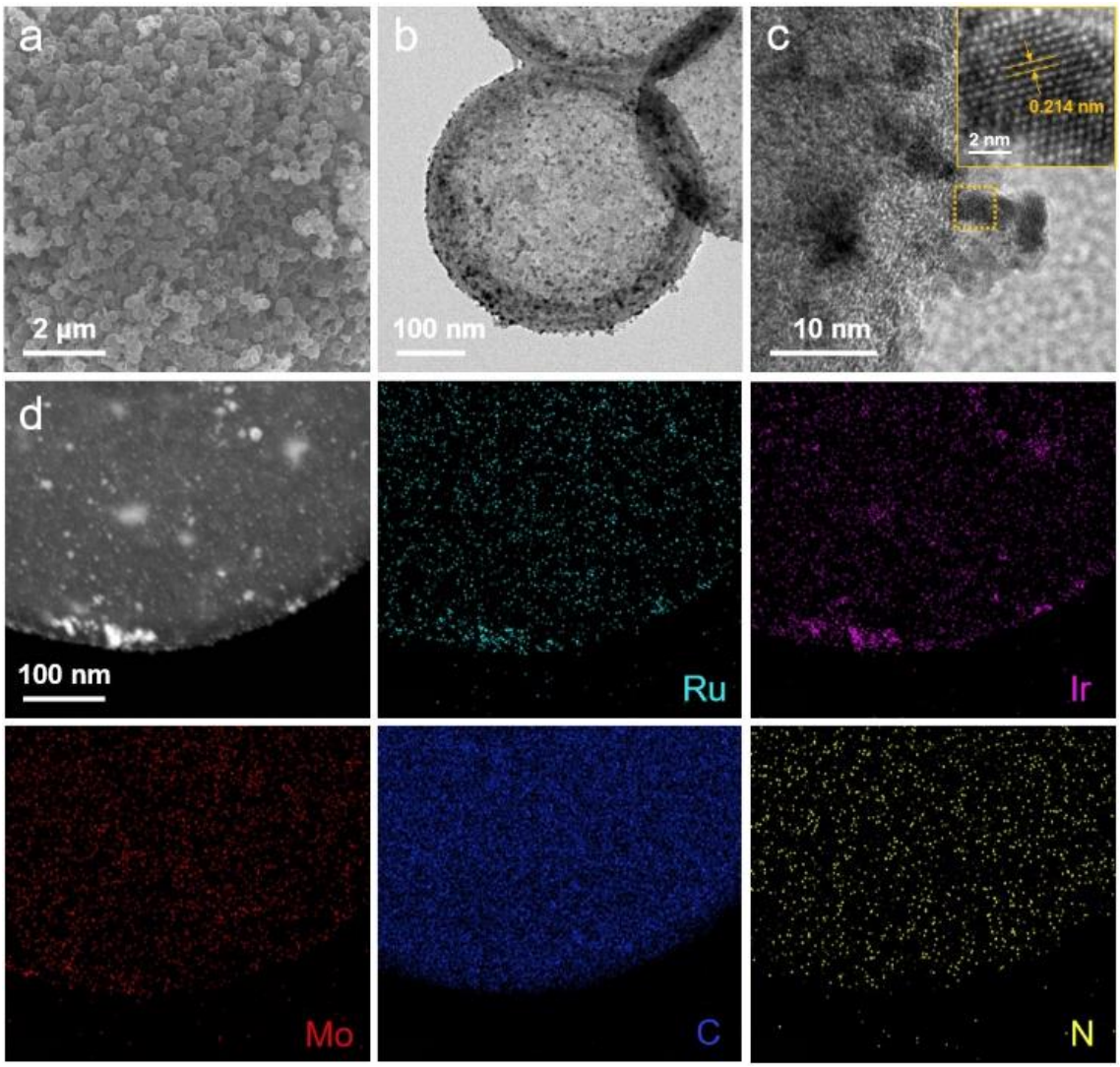

Figure 1. *(a) SEM, (b, c) TEM, and (d) EDS mapping of RuIrMo@MHCS.*

XRD patterns (Figure 2) of RuIrMo@MHCS, NbIrMo@MHCS, and IrMo@MHCS exhibit characteristic peaks at 2θ ≈ 41°, 47°, 69°, 83°, and 88°, indexed to the (111), (200), (220), (311), and (222) planes of FCC Ir (PDF#87-0715). No distinct peaks for metallic Mo, Ru, or Nb are observed, confirming the formation of single-phase solid solutions [20].

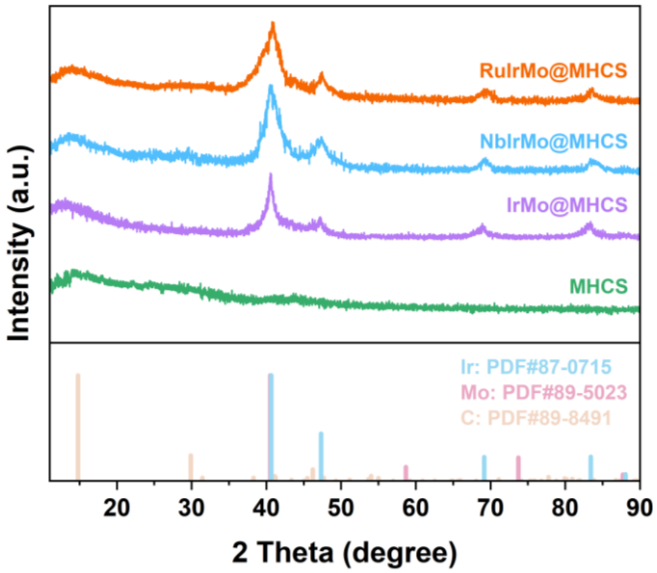

Figure 2. *XRD patterns of RuIrMo@MHCS, NbIrMo@MHCS, IrMo@MHCS, and MHCS.*

XPS survey spectra (Figure 3a) confirm the presence of Ir, Ru, Mo, C, and N in RuIrMo@MHCS. The high-resolution Ir 4f spectrum (Figure 3b) shows four peaks at 61.7, 62.8, 64.7, and 65.9 eV, assigned to Ir^0 $4f_{7/2}$, Ir^{4+} $4f_{7/2}$, Ir^0 $4f_{5/2}$, and Ir^{4+} $4f_{5/2}$, respectively. Notably, the Ir 4f peaks in RuIrMo@MHCS are shifted to higher binding energy compared to IrMo@MHCS, indicating electron transfer from Ir to Ru. Conversely, NbIrMo@MHCS shows a lower binding energy shift, suggesting electron enrichment around Ir. This directional electron transfer is expected to create abundant HOR active sites and optimize intermediate adsorption energies.

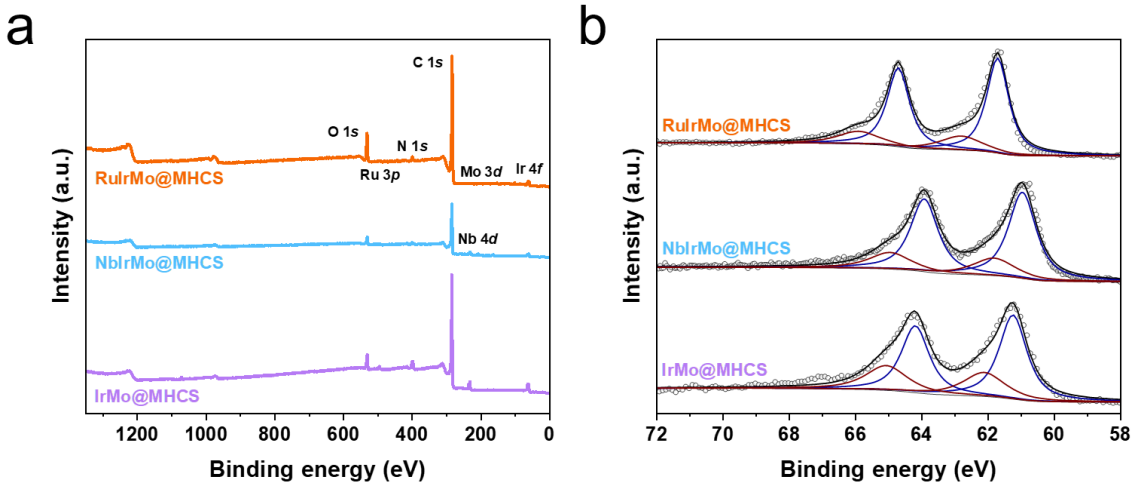

Figure 3. *(a) XPS survey spectra and (b) Ir 4f XPS spectra of RuIrMo@MHCS, NbIrMo@MHCS, and IrMo@MHCS.*

4.2. Alkaline HOR Electrocatalytic Performance

The HOR polarization curves measured at 1600 rpm in H_2-saturated 0.1 M KOH (Figure 4) show that RuIrMo@MHCS exhibits the fastest increase in anodic current with potential and reaches a limiting current plateau at ~0.15 V, indicative of superior alkaline HOR activity. Both ternary alloys outperform the binary IrMo@MHCS and commercial Pt/C.

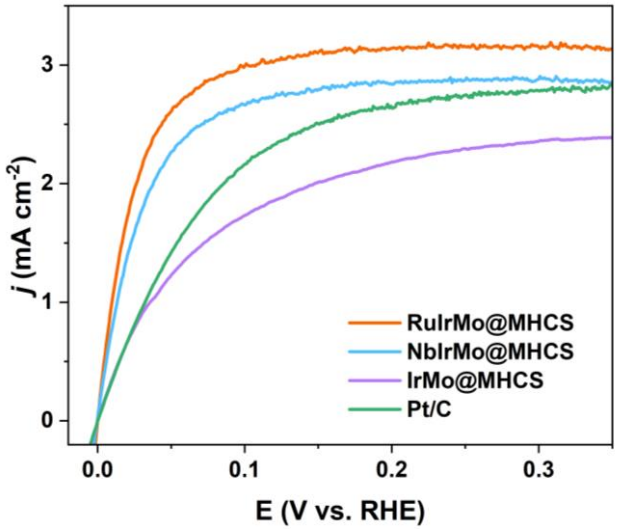

Figure 4. *HOR polarization curves of RuIrMo@MHCS, NbIrMo@MHCS, IrMo@MHCS, and commercial Pt/C in H_2-saturated 0.1 M KOH (1600 rpm, 1 mV s^{-1}).*

The HOR polarization curves of the samples at a scan rate of 1 mV s^{-1} and rotational speeds of 400 rpm, 900 rpm, 1600 rpm, 2500 rpm, and 3600 rpm are shown in Figure 5. It has been demonstrated that, owing to accelerated H_2 transport, the limiting current density of various catalysts exhibits a marked increase with rising rotational speed.

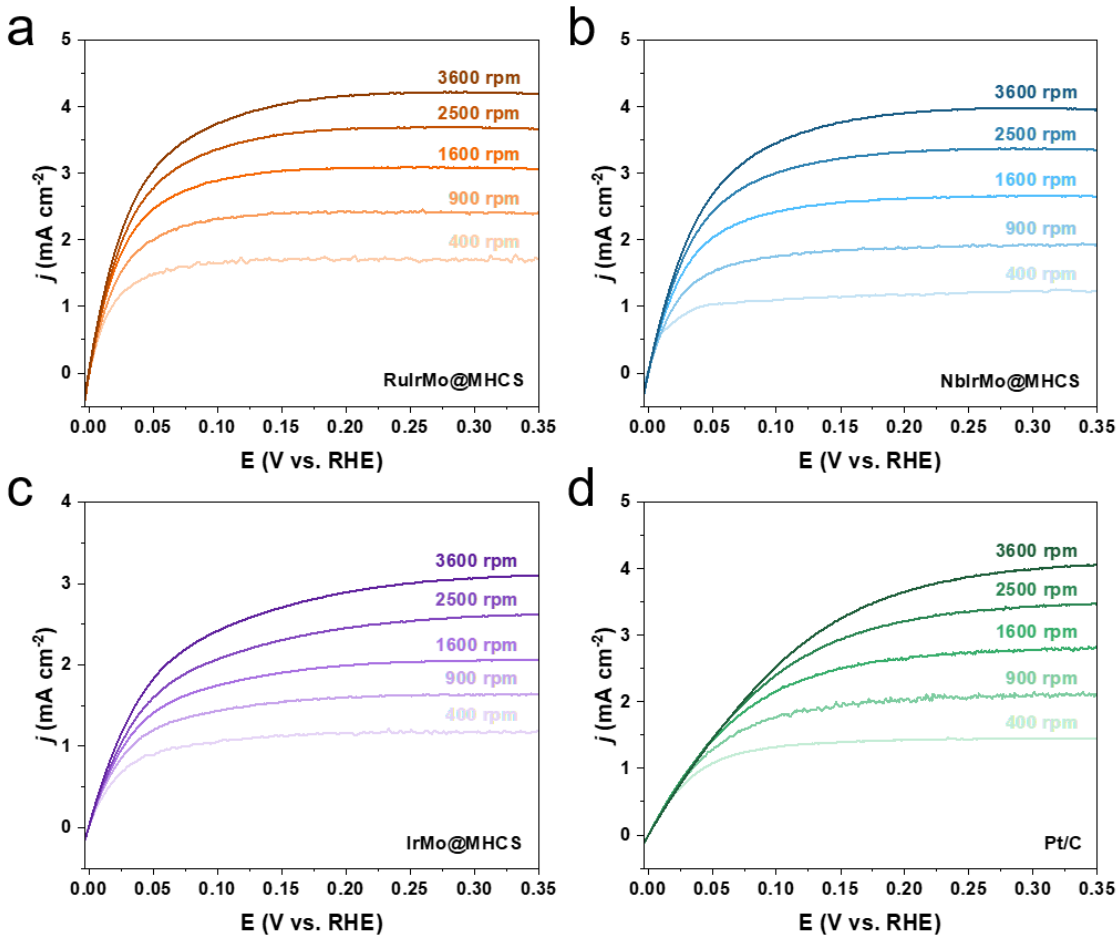

Figure 5. *HOR polarization curves of (a) RuIrMo@MHCS, (b) NbIrMo@MHCS, (c) IrMo@MHCS, and (d) commercial 20 wt.% Pt/C at different rotation speeds.*

The kinetic current densities (j_k) extracted from Levich analysis (Figure 6a) demonstrate that RuIrMo@MHCS consistently gives higher values across all potentials. Fitting the micro-polarization region using the Butler–Volmer equation (Figure 6b) yields exchange current densities (j_0) of 6.79, 4.07, 1.23, and 1.20 mA cm^{-2} for RuIrMo@MHCS, NbIrMo@MHCS, IrMo@MHCS, and Pt/C, respectively. At 50 mV overpotential, RuIrMo@MHCS achieves a j_k of 18.04 mA cm^{-2} (Figure 6c), which is 1.55, 6.96, and 6.14 times higher than those of NbIrMo@MHCS (11.61 mA cm^{-2}), IrMo@MHCS (2.59 mA cm^{-2}), and Pt/C (2.94 mA cm^{-2}). The j_0 values follow a similar trend, with RuIrMo@MHCS showing a 5.66-fold enhancement over Pt/C. As demonstrated in Figure 6d, stability tests indicate that RuIrMo@MHCS demonstrates the slowest current density decay of all the catalysts, thereby suggesting enhanced operational stability.

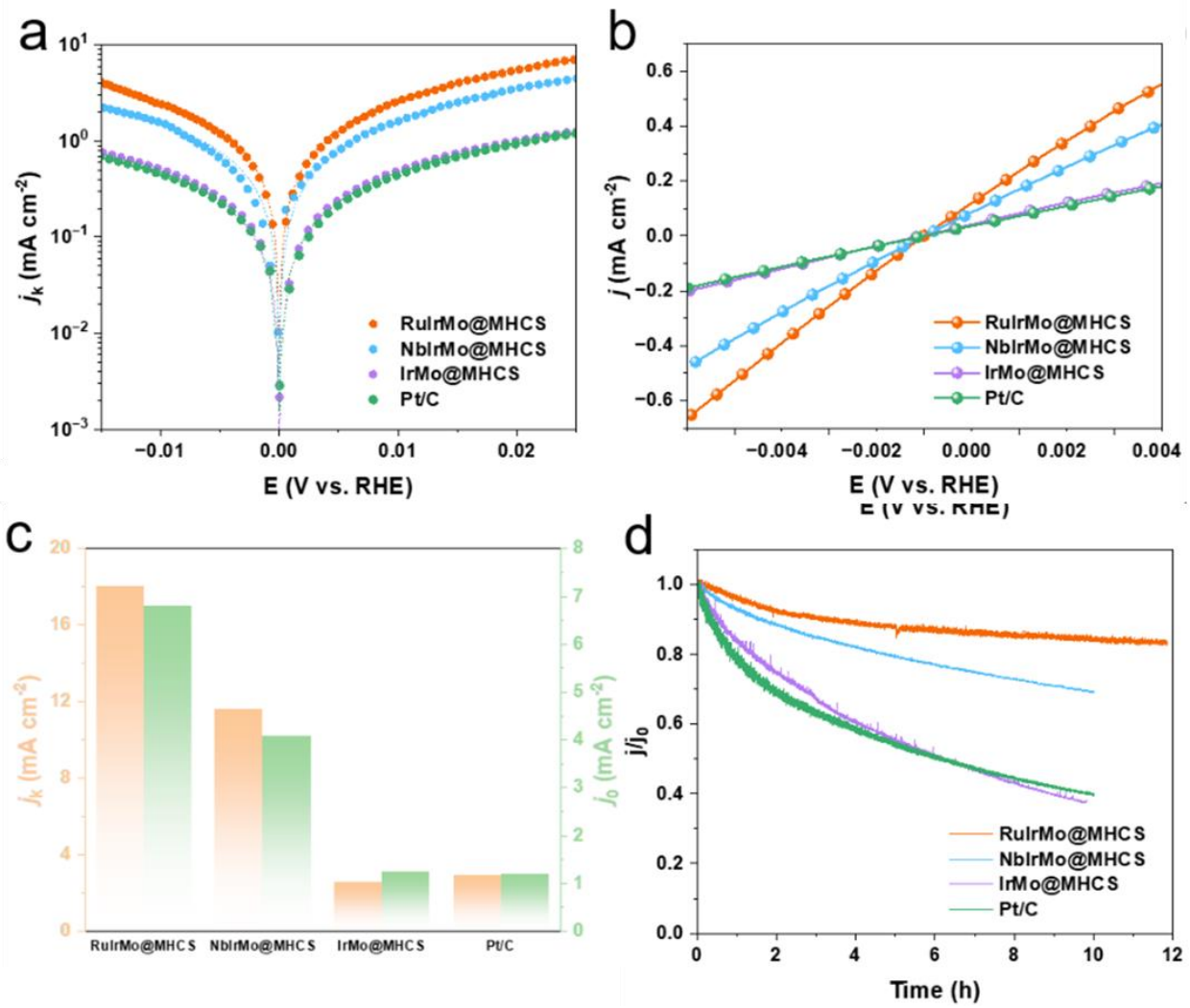

Figure 6. *(a) j_k versus potential; (b) Micro-polarization region fitting; (c) Comparison of j_k at 50 mV and j_0; (d) Chronoamperometric stability at 0.05 V.*

Zeta potential measurements were performed to evaluate the adsorption capacity of different samples for OH-. In comparison with Pt/C (−23.2 mV, see Figure 7a) and IrMo@MHCS (−36.8 mV), RuIrMo@MHCS (−38.1 mV) and NbIrMo@MHCS (−41.5 mV) exhibit more positive zeta potential values. This finding indicates that metal doping enhances their adsorption affinity for OH−. Among these, RuIrMo@MHCS exhibits a moderate OH* binding strength—weaker than NbIrMo@MHCS but stronger than Pt/C and IrMo alloys. The Hupd peak positions measured by CV (Figure 7b) can be used to qualitatively evaluate the HBE. RuIrMo@MHCS exhibits the lowest Hupd peak potential among all samples, indicating the weakest HBE. The findings suggest that the optimized H* and OH* adsorption strengths on RuIrMo@MHCS are pivotal to its exceptional basic HOR activity.

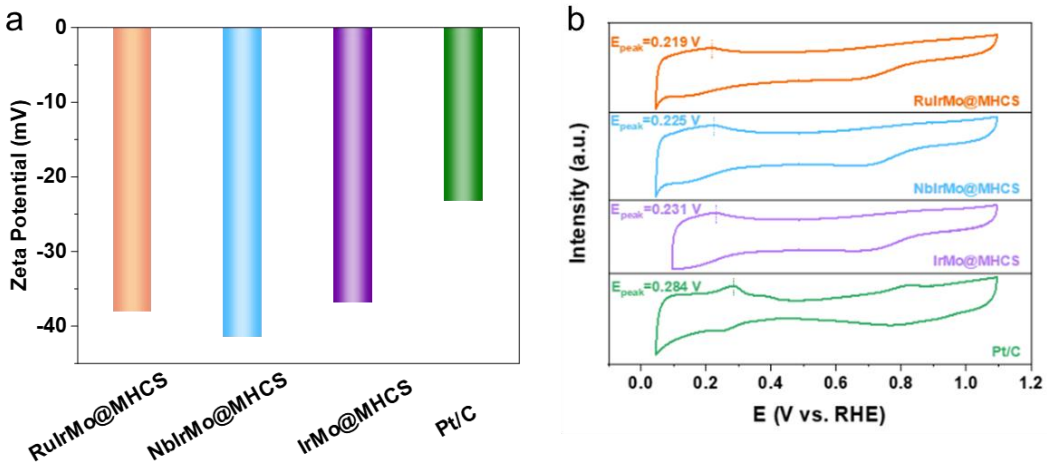

Figure 7. (a) Zeta potential; (b) Cyclic voltammograms in N_2-saturated 0.1 M KOH.

4.3. Mechanistic Investigation

DFT calculations were performed to elucidate the atomic-scale adsorption mechanism. The theoretical model of RuIrMo is shown in Figure 8a. The calculated ΔG_{H^*} for RuIrMo is –0.38 eV, significantly higher (weaker adsorption) than for NbIrMo (–0.60 eV) and IrMo (–0.58 eV) (Figure 8b). Figure 8c compares the binding energies of OH* on the different Ir-based alloys. Nb doping simultaneously strengthens both H* and OH* adsorption. In contrast, Ru doping weakens H* adsorption while moderately enhancing OH* adsorption – a combination that is beneficial for balancing the two requirements of alkaline HOR.

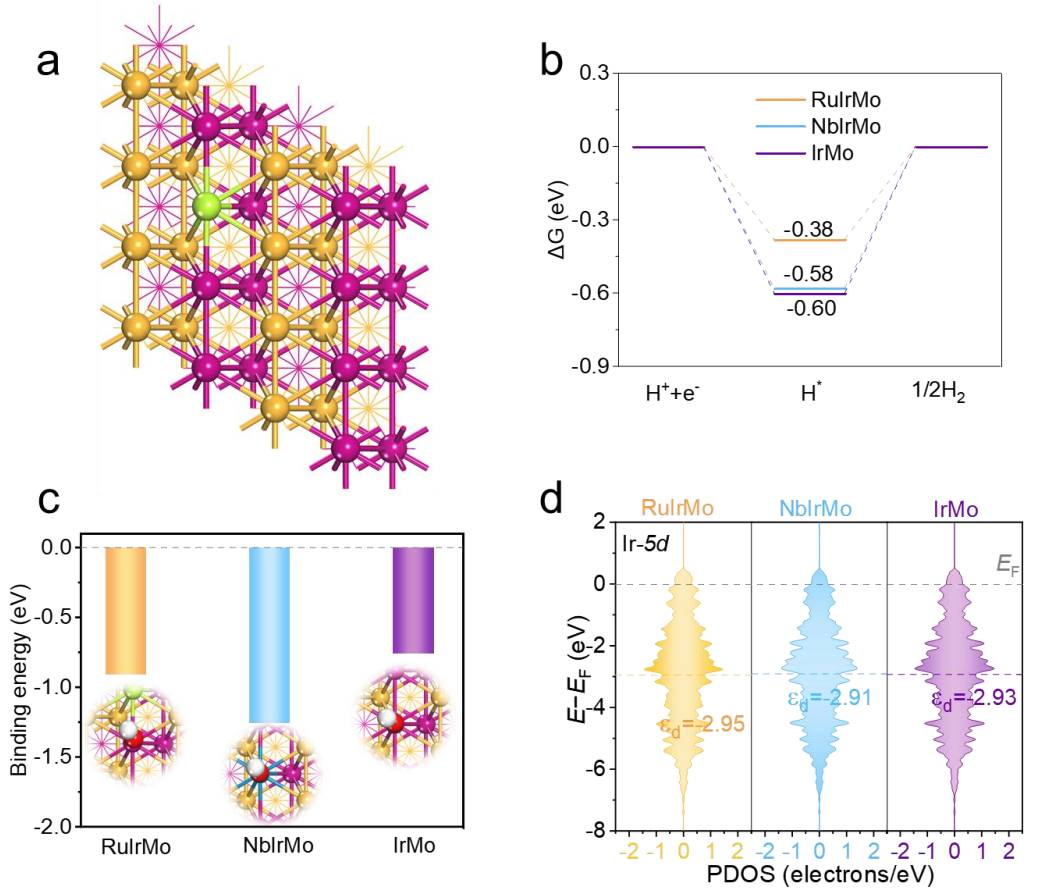

Figure 8. (a) Theoretical structural model of RuIrMo; (b) ΔG_{H^*} values; (c) OH binding energies; (d) Projected density of states (PDOS) of Ir-d orbitals.*

PDOS analysis (Figure 8d) shows that the d-band center of Ir in RuIrMo is downshifted to –2.95 eV relative to the Fermi level, compared to –2.93 eV for IrMo and –2.91 eV for NbIrMo. A downshifted d-band center typically weakens adsorbate binding. This electronic effect explains the moderate H* adsorption on RuIrMo, bringing ΔG_{H^*} close to the optimum and thereby accelerating the HOR kinetics. Meanwhile, the presence of Ru provides additional OH* adsorption sites, facilitating the Volmer step.

5. Conclusions

In summary, we have developed a multicomponent RuIrMo@MHCS catalyst that effectively breaks the linear scaling relationship between H* and OH* adsorption energies for alkaline HOR. The catalyst forms a single-phase FCC solid solution with uniformly dispersed nanoparticles on hollow carbon spheres. Ru doping induces electron transfer from Ir to Ru, downshifting the Ir d-band center and resulting in weakened H* adsorption (ΔG_{H^*} = –0.38 eV) while preserving strong OH* adsorption on Mo sites. Consequently, RuIrMo@MHCS delivers a kinetic current density of 18.04 mA cm^{-2} and an exchange current density of 6.79 mA cm^{-2} at 50 mV overpotential, outperforming commercial Pt/C by factors of 6.14 and 5.66, respectively, with excellent stability. This work demonstrates that multicomponent alloying is a viable strategy for decoupling and synergistically optimizing the adsorption of reaction intermediates, providing a rational design pathway for efficient alkaline HOR catalysts.

Abbreviations

HOR	Hydrogen Oxidation Reaction
AEMFC	Anion-exchange Membrane Fuel Cells
ΔG_{H^*}	Hydrogen Adsorption Free Energy
HBE	Hydrogen Binding Energy
OHBE	Hydroxyl Binding Energy
MHCS	Mesoporous Hollow Carbon Spheres
DFT	Density Functional Theory
XRD	X-ray Diffraction
SEM	Scanning Electron Microscopy
TEM	Transmission Electron Microscopy
XPS	X-ray Photoelectron Spectroscopy
EDS	Energy-dispersive X-ray Spectroscopy
RDE	Rotating Disk Electrode
CV	Cyclic Voltammetry
RHE	Reversible Hydrogen Electrode
j_k	Kinetic Current Density
j_0	Exchange Current Density

Author Contributions

Yanfu Tong: Conceptualization, Formal Analysis, Resources, Writing – original draft

Xuejin Li: Data curation, Funding acquisition, Methodology, Project administration

Wei Xing: Methodology, Supervision, Writing – review & editing

Funding

This work is supported by the Young Taishan Scholars Program of Shandong Province (tsqn202211082), the Natural Science Foundation of Shandong Province (ZR2023MB051, ZR2024QE082), National Natural Science Foundation of China (52277229, 52573362), the CNPC Innovation Foundation (2022DQ02-0410), the Taishan Industrial Experts Program, and the Fundamental Research Funds for the Central Universities (No. 26CX04033A).

Data Availability Statement

The data is available from the corresponding author upon reasonable request.

Conflicts of Interest

The authors declare no conflicts of interest.

References

[1] Wang C, Wang P, Shi H, Yang J, Meng P, Yang Y, et al. Accelerating Kinetics of Alkaline Hydrogen Oxidation Reaction on Ru through Engineering Oxophilicity. ACS Materials Letters 2024; 6(10): 4491-4497. https://doi.org/10.1021/acsmaterialslett.4c01346

[2] Park J, Kim H, Kim S, Yi SY, Min H, Choi D, et al. Boosting Alkaline Hydrogen Oxidation Activity of Ru Single-Atom Through Promoting Hydroxyl Adsorption on Ru/WC_{1-x} Interfaces. Advanced Materials 2024; 36(4): 2308899. https://doi.org/10.1002/adma.202308899

[3] Li M, Xie Z, Zheng X, Li L, Li J, Ding W, et al. Revealing the Regulation Mechanism of Ir–MoO_2 Interfacial Chemical Bonding for Improving Hydrogen Oxidation Reaction. ACS Catalysis 2021; 11(24): 14932-14940. https://doi.org/10.1021/acscatal.1c04440

[4] Durst J, Siebel A, Simon C, Hasché F, Herranz J, Gasteiger HA. New Insights Into the Electrochemical Hydrogen Oxidation and Evolution Reaction Mechanism. Energy & Environmental Science 2014; 7(7): 2255-2260. https://doi.org/10.1039/C4EE00440J

[5] Yang X, Ouyang B, Shen P, Sun Y, Yang Y, Gao Y, et al. Ru Colloidosome Catalysts for the Hydrogen Oxidation Reaction in Alkaline Media. Journal of the American Chemical Society 2022; 144(25): 11138-11147. https://doi.org/10.1021/jacs.2c00793

[6] Wang X, Tong Y, Feng W, Liu P, Li X, Cui Y, et al. Embedding Oxophilic Rare-earth Single Atom in Platinum Nanoclusters for Efficient Hydrogen Electro-oxidation. Nature Communications 2023; 14(1): 3767. https://doi.org/10.1038/s41467-023-39475-5

[7] Shi H, Dai T-Y, Sun X-Y, Zhou Z-L, Zeng S-P, Wang T-H, et al. Dual-Intermetallic Heterostructure on Hierarchical Nanoporous Metal for Highly Efficient Alkaline Hydrogen Electrocatalysis. Advanced Materials 2024; 36(38): 2406711. https://doi.org/10.1002/adma.202406711

[8] Jin Y, Fan X, Cheng W, Zhou Y, Xiao L, Luo W. The Role of Phosphorus on Alkaline Hydrogen Oxidation Electrocatalysis for Ruthenium Phosphides. Angewandte Chemie International Edition 2024; 136(41): e202406888. https://doi.org/10.1002/anie.202406888

[9] Tong Y, Xu J, Ding Y, Kong W, Li B, Wang J, et al. Theoretical Insights into the Hydrogen Oxidation Reaction on Single Metal Atoms Anchored on the Edge of MoS_2 Nanosheets. Computational Materials Science 2023; 218(1): 111921. https://doi.org/10.1016/j.commatsci.2022.111921

[10] Qin S, Duan Y, Zhang XL, Zheng LR, Gao FY, Yang PP, et al. Ternary Nickel-tungsten-copper Alloy Rivals Platinum for Catalyzing Alkaline Hydrogen Oxidation. Nature Communications 2021; 12(1): 2686. https://doi.org/10.1038/s41467-021-22996-2

[11] Yao Z-C, Tang T, Jiang Z, Wang L, Hu J-S, Wan L-J. Electrocatalytic Hydrogen Oxidation in Alkaline Media: From Mechanistic Insights to Catalyst Design. ACS Nano 2022; 16(4): 5153-5183. https://doi.org/10.1021/acsnano.2c00641

[12] Wang Y, Sun L, Lv H, Zheng C, Liu B. Ordered Mesoporous Intermetallic PtP_2 Nanoparticles with Enhanced Electrocatalytic Activity and Stability for Hydrogen Evolution. CCS Chemistry 2023; 5(8): 1896-1907. https://doi.org/10.31635/ccschem.022.202202451

[13] Tong Y, Li X, Wang X, Zhao L, Luo W, Huang Z, et al. Entropy-Mediated Gradient Oxygenophilic Architecture on High-Entropy Alloy for Dynamic Spillover and Bifunctional Hydrogen Electrocatalysis. Advanced Materials 2026; 38(9): e17450. https://doi.org/10.1002/adma.202517450

[14] Men Y, Wu D, Hu Y, Li L, Li P, Jia S, et al. Understanding Alkaline Hydrogen Oxidation Reaction on PdNiRuIrRh High-Entropy-Alloy by Machine Learning Potential. Angewandte Chemie International Edition 2023; 62(27): e202217976. https://doi.org/10.1002/anie.202217976

[15] Tang T, Liu X, Luo X, Xue Z, Pan H-R, Fu J, et al. Unconventional Bilateral Compressive Strained Ni–Ir Interface Synergistically Accelerates Alkaline Hydrogen Oxidation. Journal of the American Chemical Society 2023; 145(25): 13805-13815. https://doi.org/10.1021/jacs.3c02487

[16] Qin B, Yu H, Jia J, Jun C, Gao X, Yao D, et al. A Novel IrNi@PdIr/C Core–shell Electrocatalyst with Enhanced Activity and Durability for the Hydrogen Oxidation Reaction in Alkaline Anion Exchange Membrane Fuel Cells. Nanoscale 2018; 10(10): 4872-4881. https://doi.org/10.1039/C7NR09452C

[17] Ma X, Zhang S, Zhou Y, Lei W, Zhai Y, Zhao Y, et al. PtIrFeCoNiMo High-entropy Alloy Nanodendrites for Boosting the Alkaline Hydrogen Oxidation Performance. Journal of Materials Chemistry A 2024; 12(15): 8862-8868. https://doi.org/10.1039/D3TA06817J

[18] Liu D-Q, Luo Z, Zhang B, Zhao G, Guo W, Chen J, et al. Tailoring Interfacial Charge Transfer of Epitaxially Grown Ir Clusters for Boosting Hydrogen Oxidation Reaction. Advanced Energy Materials 2023; 13(1): 2202913. https://doi.org/10.1002/aenm.202202913

[19] Chen Z, Zeng H, Zhang C, Cai H, Jiang Y, Hu J, et al. Ru–Mo Solid–solution Catalyst for Hydrogen Evolution in Alkaline Electrolyte. Nano Research 2025; 18(5): 94907346. https://doi.org/10.26599/NR.2025.94907346

[20] Fang J, Wang H, Dang Q, Wang H, Wang X, Pei J, et al. Atomically Dispersed Iridium on Mo_2C as An Efficient and Stable Alkaline Hydrogen Oxidation Reaction Catalyst. Nature Communications 2024; 15(1): 4236. https://doi.org/10.1038/s41467-024-48672-9